ACS APPLIED MATERIALS & INTERFACES

www.acsami.org

Research Article

Unconventional Substitution for $BiVO_4$ to Enhance Photoelectrocatalytic Performance by Accelerating Polaron Hopping

Jiachen Wang, Jing Bai,* Yan Zhang, Lei Li, Changhui Zhou, Tingsheng Zhou, Jinhua Li, Hong Zhu, and Baoxue Zhou*

Cite This: https://doi.org/10.1021/acsami.2c23169

Read Online

ACCESS | Metrics & More | Article Recommendations | Supporting Information

ABSTRACT: Bismuth vanadate ($BiVO_4$) as a fascinating semiconductor for photoelectrocatalytic (PEC) water oxidation with suitable band gap (E_g) has been limited by the issue of poor separation and transportation of charge carriers. Herein, we propose an unconventional substitution of V^{5+} sites by Ti^{4+} in $BiVO_4$ (Ti:$BiVO_4$) for the similar ionic radii and accelerated polaron hopping. Ti:$BiVO_4$ increased the photocurrent density 1.90 times up to 2.51 mA cm^{-2} at 1.23 V vs RHE and increased the charge carrier density 1.81 times to 5.86×10^{18} cm^{-3}. Compared with bare $BiVO_4$, Ti:$BiVO_4$ improves the bulk separation efficiency to 88.3% at 1.23 V vs RHE. The DFT calculations have illustrated that Ti-doping modification could decrease the polaron hopping energy barrier, narrow the E_g, and decrease the overpotential of the oxygen evolution reaction (OER) concurrently. With further spin-coated FeOOH cocatalyst, the photoanode has a photocurrent density of 3.99 mA cm^{-2} at 1.23 V vs RHE. The excellent PEC performance of FeOOH/Ti:$BiVO_4$ is attributed to the synergistic effect of the FeOOH layer and Ti doping, which could promote charge carrier separation and transfer by expediting polaron migration.

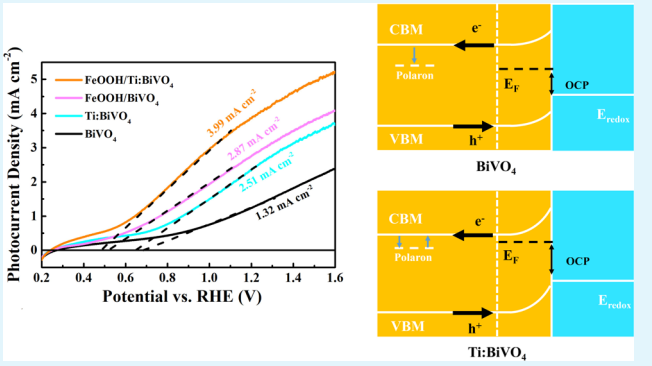

KEYWORDS: *bismuth vanadate ($BiVO_4$), Ti-doped $BiVO_4$, photoelectrocatalytic, polaron hopping, density function theory (DFT)*

INTRODUCTION

Conversion of solar energy to a sustainable pattern by photoelectrocatalytic (PEC) technology has become one of the most fascinating strategies.[1−3] Among various semiconductors, the scheelite bismuth vanadate ($BiVO_4$) is prospective for PEC water oxidation and degradation of pollutants, with good stability, nontoxicity, and proper band gap (~2.4 eV).[4] However, pristine $BiVO_4$ suffers from severe photogenerated holes recombination resulting in low charge separation and transfer efficiency for the short hole-diffusion length and the low carrier mobility.[5] To overcome the above disadvantages, researchers have reported a variety of methods for $BiVO_4$, such as introducing oxygen vacancies,[6−10] constructing heterojunction,[11−13] and element doping.[14−19]

Among the above methods, doping $BiVO_4$ with ions is an efficient way to accelerate the charge transfer kinetics and increase the conductivity of photoanodes. W^{6+}- and Mo^{6+}-doped $BiVO_4$ could effectively increase the major carrier density and enhance PEC water splitting.[20,21] P-doped $BiVO_4$ significantly promotes charge transfer kinetics with a remarkable increase of photocurrent density.[22] Substituting V^{5+} could suppress bulk recombination with improved electron mobility, which is attributed to the decreased polaron hopping energy barrier by the local polarization of the lattice.[23,24] The conventional substitution of V^{5+} involves doping with higher valent metal ions (W^{6+} or Mo^{6+}),[20,21] but there are few studies on the doping with lower valent metal ions, for example, Ti^{4+}, which has been doped into $BiVO_4$ for photocatalysis rather than photo-electrocatalysis.[25,26]

Here, we propose an unconventional substitution of V^{5+} sites by lower valent Ti^{4+} ions with the similar ionic radii to synthesize the Ti:$BiVO_4$ photoanode, which increases the photocurrent density 1.90 times up to 2.51 mA cm^{-2} at 1.23 V vs RHE and increases the charge carrier density 1.81 times to 5.86×10^{18} cm^{-3}, compared with bare $BiVO_4$. In addition, the Ti:$BiVO_4$ improves the bulk separation efficiency to 88.3% at 1.23 V vs RHE, much higher than that of $BiVO_4$ (60.1%). The DFT calculations reveal that the incorporation of Ti^{4+} for $BiVO_4$ photoanode could lower the polaron hopping activation

Received: December 27, 2022
Accepted: February 27, 2023

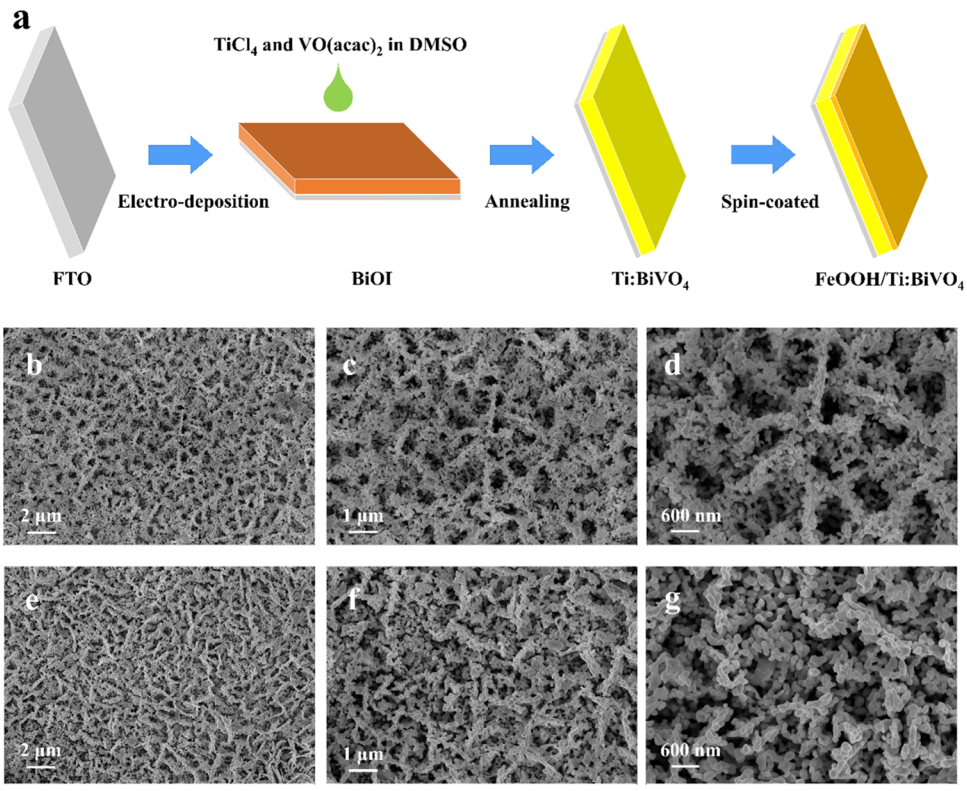

Figure 1. (a) Schematic illustration of FeOOH/TiBiVO$_4$ photoanode synthesis; (b–d) top-view SEM images of BiVO$_4$ and (e–g) top-view SEM images of Ti:BiVO$_4$.

barrier, narrow the E_g, and decrease the overpotential of the oxygen evolution reaction (OER). With further introduction of FeOOH oxygen evolution catalysts (OECs), FeOOH/Ti:BiVO$_4$ has a photocurrent density of 3.99 mA cm^{-2} at 1.23 V vs RHE. The improved photocurrent density of FeOOH/Ti:BiVO$_4$ suggests the synergistic effect of oxygen evolution catalyst and Ti doping, which could promote charge carrier transfer and accelerate polaron hopping.

EXPERIMENTAL SECTION

Synthesis of BiVO$_4$ and Ti:BiVO$_4$ Films. KI (3.32 g) and 0.97 g of Bi(NO$_3$)$_3$·5H$_2$O were dissolved in 50 mL of deionized water with pH adjusted to ∼1.7 through HNO$_3$ as the precursor solution. Then, 0.54 g of *p*-benzoquinone dissolved in 20 mL of absolute ethanol was added into the precursor solution to obtain the clear electrodeposition solution. The BiOI layer was electrodeposited on the fluorine-doped tin oxide (FTO) in a three-electrode cell under −0.1 V vs Ag/AgCl. The BiOI layer was covered with a dimethyl sulfoxide (DMSO) solution containing 20 mM vanadyl acetylacetonate [VO(acac)$_2$], and then it was placed in a muffle furnace at 450 °C for 2 h. For Ti:BiVO$_4$, 0.05% (volume percentage) titanium tetrachloride (TiCl$_4$) ethanol solution was dropped in the DMSO solution, and annealing was carried out in the same condition as BiVO$_4$. The BiVO$_4$ and Ti:BiVO$_4$ samples were dipped in 1 M NaOH solution for 30 min to obtain BiVO$_4$ and Ti:BiVO$_4$ films without residual V_2O_5.

Preparation of the FeOOH/Ti:BiVO$_4$ Photoanode. The precursor of FeOOH, containing 20 mM FeCl$_3$ and 40 mM NaNO$_3$, was dripped on the Ti:BiVO$_4$ films for spin-coating at 1000 rpm for 10 s. Then, the film was heated under 200 °C for 10 min to obtain the FeOOH/Ti:BiVO$_4$ photoanode.

Material Characterization. The crystalline structure was characterized through X-ray diffraction (XRD) with an AXS-8 Advance (Bruker, Germany). Scanning electron microscopy (SEM) was performed with a Zeiss SUPRA55-VIP. High-resolution transmission electron microscopy (HRTEM) was performed with a Talos F200X. X-ray photoelectron spectroscopy (XPS) was performed with an AXIS Ultra DLD (Kratos, Japan). The UV–vis spectra were collected using a TU-1901 spectrophotometer. Atomic force microscopy (AFM) was performed with a Bruker Dimension ICON. Density functional theory (DFT) calculations are illustrated in the Supporting Information.

Photoelectrochemical Measurements. PEC measurements were performed using a CHI 660e electrochemical workstation in a three-electrode system with a 0.2 M Na$_2$SO$_4$ under an AM 1.5G solar power system (100 mW cm^{-2}) with a 300 W Xe lamp (PLS-SXE300/300UV, Perfect Light). Linear sweep voltammetry (LSV) plots were examined at a scan rate of 50 mV s^{-1}. The conversion of potential vs Ag/AgCl ($E_{Ag/AgCl}$) to reversible hydrogen electrode (E_{RHE}) is according to eq 1

$$E_{RHE} = E_{Ag/AgCl} + 0.0591\ V \times pH + 0.1976 \quad (1)$$

The incident photon-to-current efficiencies (IPCEs) were examined in a three-electrode cell at 1.23 V vs RHE, with the monochromatic wavelength from 400 to 600 nm. Electrochemical impedance spectroscopy (EIS) was characterized at the frequency from 0.1 Hz to 100 kHz. Intensity-modulated photocurrent/photovoltage spectroscopy (IMPS/IMVS) was implemented using a Zahner CIMPS-2 system.

RESULTS AND DISCUSSION

Synthesis and Characterization. The preparation procedure of the FeOOH/Ti:BiVO$_4$ photoanode is illustrated in Figure 1a, by electrodeposition, annealing, and spin-coating. The BiOI was electrochemically deposited on the FTO, and then a DMSO solution of [VO(acac)$_2$] without/with TiCl$_4$ was dripped onto BiOI and annealed in air to fabricate BiVO$_4$ and Ti:BiVO$_4$. As seen in the top-view SEM images in Figure 1b–d, BiVO$_4$ films have uniformly grown in the shape of nanorods. After the doping of titanium, there were no significant morphology changes in the SEM images of

https://doi.org/10.1021/acsami.2c23169
ACS Appl. Mater. Interfaces XXXX, XXX, XXX–XXX

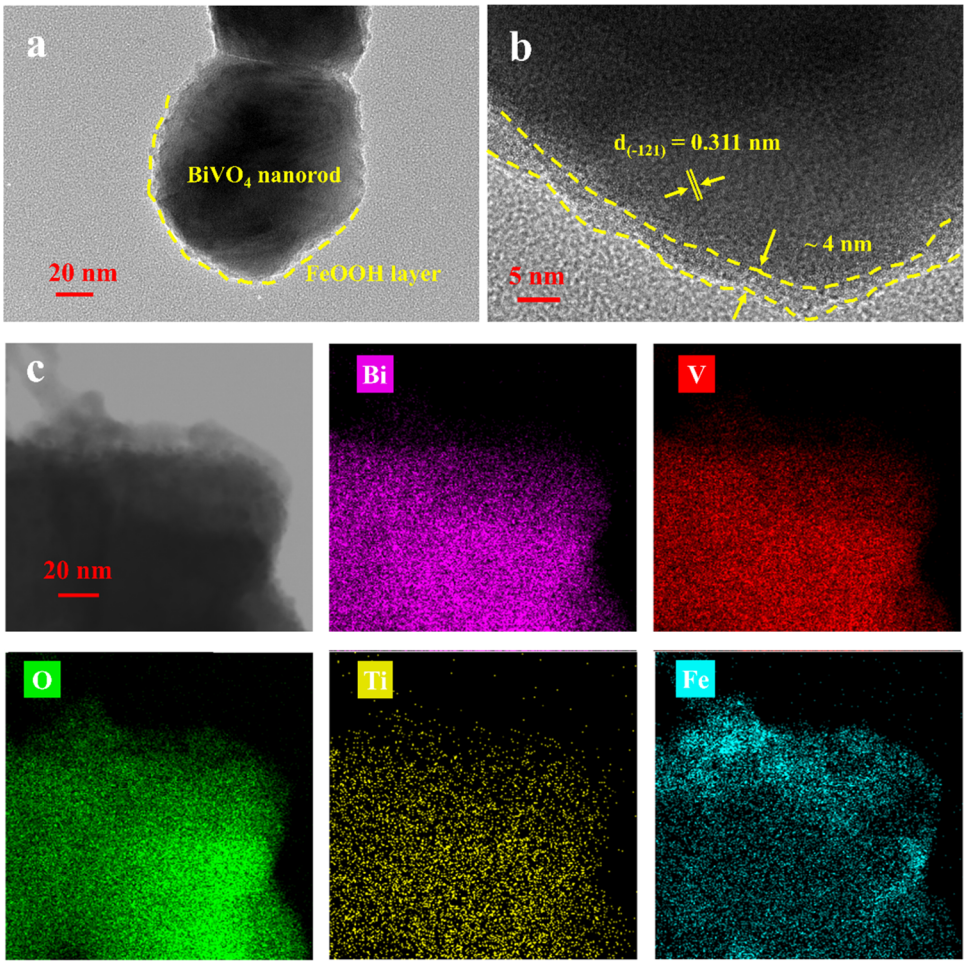

Figure 2. (a, b) TEM images of FeOOH/Ti:$BiVO_4$, and (c) TEM elemental mappings for Bi, V, O, Ti, and Fe.

Ti:$BiVO_4$ (Figure 1e–g). The FeOOH layer was spin-coated on the surface of Ti:$BiVO_4$ films, and the cross-sectional SEM image of FeOOH/Ti:$BiVO_4$ is shown in Figure S1 with element mapping. In Figure S2, the XRD patterns of $BiVO_4$ and Ti:$BiVO_4$ both have characteristic diffraction peaks indexed to the scheelite $BiVO_4$ (JCPDS no. 14-0688), with negligible variations.[27,28]

To further study the structural changes by Ti doping and FeOOH spin-coating, the HRTEM images of FeOOH/Ti:$BiVO_4$ are presented in Figure 2. The surface of $BiVO_4$ nanorods is uniformly covered with an amorphous FeOOH layer (Figure 2a). The *d*-spacing is equal to 0.311 nm related to the lattice plane $(\bar{1}21)$ (Figure 2b), where the thickness of the FeOOH layer is ~4 nm. The TEM images of FeOOH/$BiVO_4$ film and the AFM images of $BiVO_4$ and FeOOH/$BiVO_4$ are shown in Figures S3 and S4. The uniform distribution of Bi, V, O, Ti, and Fe is displayed in Figure 2c, confirming that Ti has been successfully doped in $BiVO_4$. The elemental mapping shows that Fe is concentrated on the top of the image, indicating the amorphous FeOOH layer coated on the surface of $BiVO_4$ nanorods (Figure 2a,b).

X-ray photoelectron spectroscopy (XPS) was performed (Figure 3) to analyze the varieties of surface valence states. The total survey spectrum and the high-resolution XPS of Fe 2p for FeOOH/Ti:$BiVO_4$ are shown in Figure S5. The total survey spectrum could detect the elements of Bi, V, O, Fe, and Ti after doping and spin-coating. In Figure 3a, the high-resolution XPS of Ti 2p for Ti:$BiVO_4$ has two characterized peaks at 465.14 and 458.20 eV, corresponding to Ti $2p_{1/2}$ and Ti $2p_{3/2}$, respectively.[25,29,30] Compared with $BiVO_4$, Ti:$BiVO_4$ has a low-energy shift of Bi 4f and V 2p (Figure 3b,c), suggesting the reduced elements for the presence of oxygen vacancies (O_V).[6,25,31] For the O 1s spectrum in Figure 3d, there are three oxygen chemical states at ~529.45, ~532.21, and ~531.25 eV for lattice oxygen (O_L), for chemisorbed O_2 and H_2O (O_C), and for O_V, respectively.[32−34] The peak area of O_V in Ti:$BiVO_4$ is larger than that of the original $BiVO_4$, attributed to the formation of oxygen vacancies. The FeOOH/$BiVO_4$ was characterized by the total XPS survey spectrum and the high-resolution XPS of Fe 2p (Figure S6).

PEC Performance. The Ti:$BiVO_4$ has been successfully synthesized, and the ratio of Ti has been optimized in Figure S7. In Figure 4a, the Ti:$BiVO_4$ has the photocurrent density (J_{PEC}) of 2.51 mA cm^{-2} at 1.23 V vs RHE higher than that of pristine $BiVO_4$ (1.32 mA cm^{-2}). In addition, the Ti-doped modification could realize a high J_{PEC} of 1.08 mA cm^{-2} at 0.90 V vs RHE for $BiVO_4$. Here, the water oxidation performance of Ti:$BiVO_4$ is better than those of the state-of-the-art doped $BiVO_4$ photoanodes at a low bias voltage (0.9 V vs RHE) and 1.23 V vs RHE without Na_2SO_3 (Table S1). With the modification of FeOOH, the J_{PEC} values of FeOOH/$BiVO_4$ and FeOOH/Ti:$BiVO_4$ are 2.90 and 3.99 mA cm^{-2} at 1.23 V vs RHE (Figure 4a), respectively. The onset potential of FeOOH/Ti:$BiVO_4$ cathodically shifted 184 mV over Ti:Bi-

https://doi.org/10.1021/acsami.2c23169
ACS Appl. Mater. Interfaces XXXX, XXX, XXX−XXX

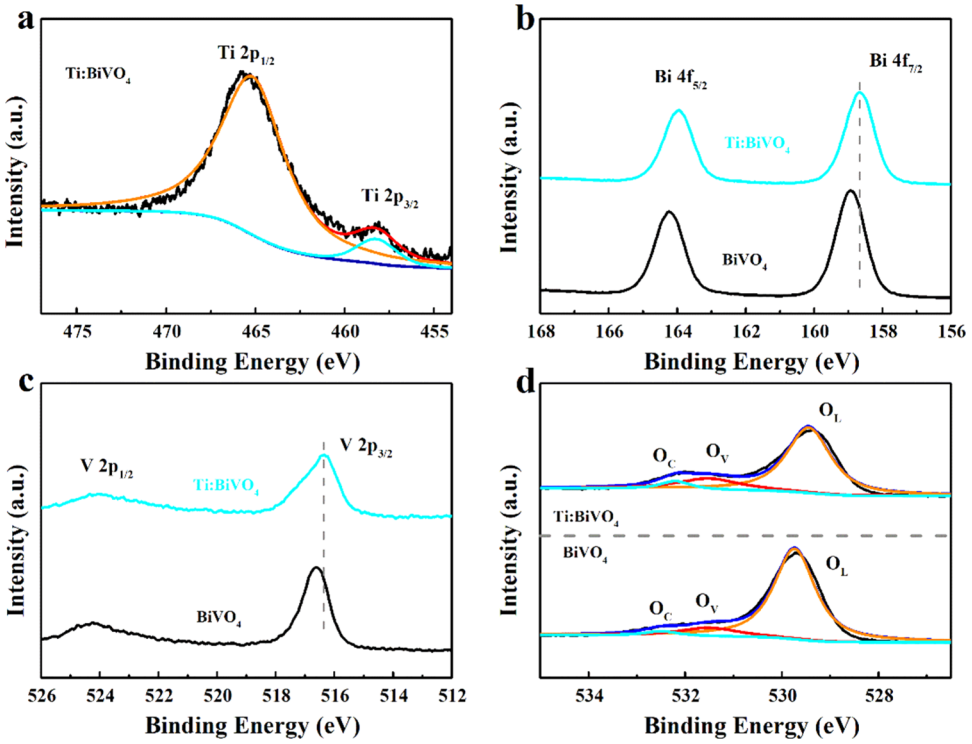

Figure 3. (a) Deconvoluted high-resolution Ti 2p XPS spectra of $Ti:BiVO_4$, (b) Bi 4f, (c) V 2p, and (d) O 1s XPS spectra for $BiVO_4$ and $Ti:BiVO_4$.

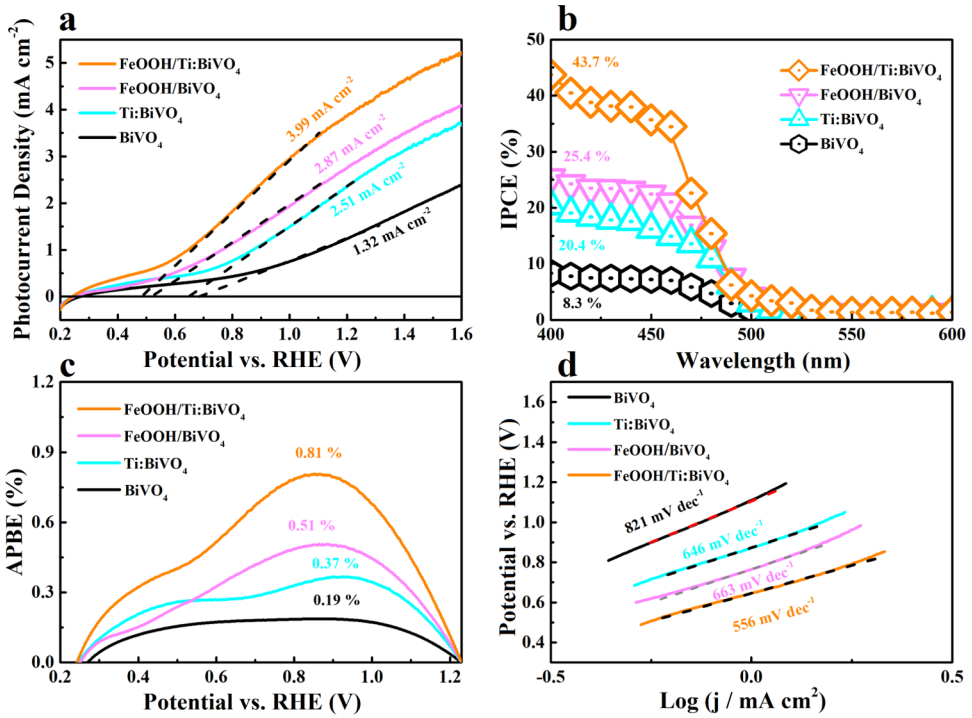

Figure 4. (a) LSV, (b) IPCE, (c) ABPE, and (d) Tafel plots for $BiVO_4$, $Ti:BiVO_4$, $FeOOH/BiVO_4$, and $FeOOH/Ti:BiVO_4$ under 100 mW cm^{-2} irradiation in 0.2 M Na_2SO_4 solution.

VO_4, due to FeOOH serving as OECs.[35] In Figure S8, the $FeOOH/Ti:BiVO_4$ has a similar cathodical shift to $FeOOH/BiVO_4$, but its photocurrent density increases 1.28 times over that of $FeOOH/BiVO_4$, indicating that Ti doping could effectively promote charge carrier transfer between FeOOH and $BiVO_4$. The chopped LSV curves of $Ti:BiVO_4$ and $BiVO_4$ with the negligible dark current are shown in Figure S9. The sharp transient spikes of $BiVO_4$ are decreased under irradiation for the Ti doping suppressing charge carrier recombination. The stability of $BiVO_4$, $FeOOH/BiVO_4$, and $FeOOH/Ti:BiVO_4$ is recorded for 2 h (Figure S10), and the $FeOOH/Ti:BiVO_4$ has a slower decay of photocurrent density

https://doi.org/10.1021/acsami.2c23169
ACS Appl. Mater. Interfaces XXXX, XXX, XXX−XXX

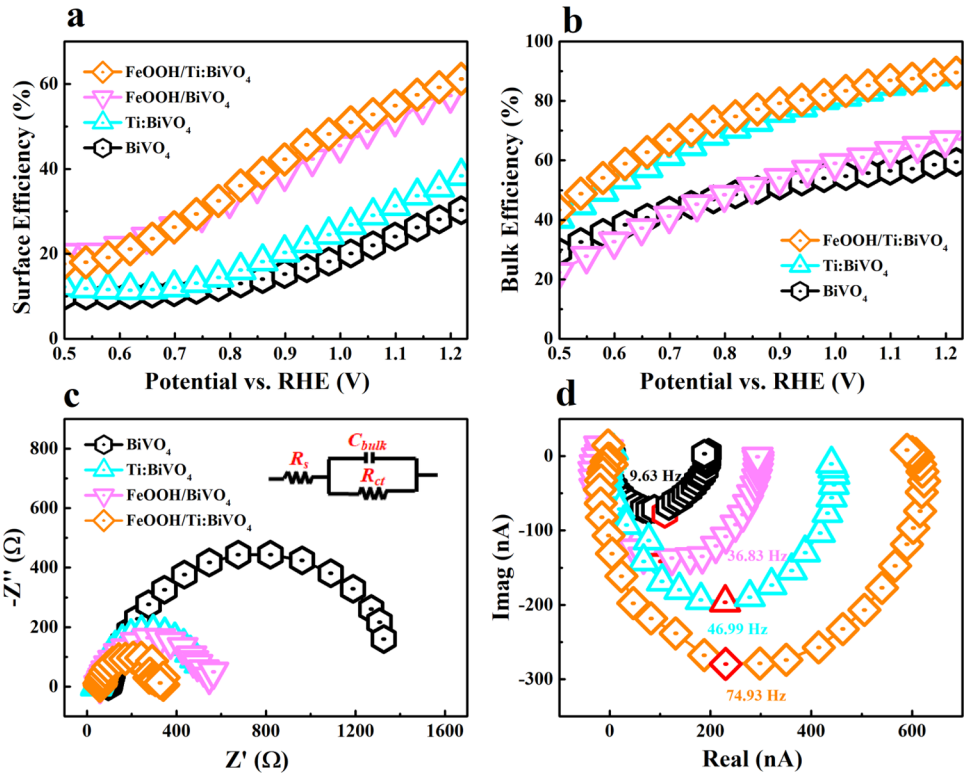

Figure 5. (a) Surface charge transfer efficiency, (b) bulk charge separation efficiency, (c) EIS Nyquist plots, and (d) IMPS plots for $BiVO_4$, $Ti:BiVO_4$, $FeOOH/BiVO_4$, and $FeOOH/Ti:BiVO_4$.

than that of $BiVO_4$ and $FeOOH/BiVO_4$. In addition, the production evolution of H_2 and O_2 and the Faradaic efficiencies of O_2 of about 95% are illustrated in Figure S11 for $FeOOH/Ti:BiVO_4$.

The IPCE curves are obtained at 1.23 V vs RHE from 400 to 600 nm as in eq 2

$$\text{IPCE}\ (\%) = (1240 \times J_{\text{mono}})/(P_{\text{mono}} \times \lambda) \tag{2}$$

where J_{mono} and P_{mono} are the photocurrent density and the light power density under the monochromatic light wavelength λ. In Figure 4b, the maximum IPCEs for $BiVO_4$, $Ti:BiVO_4$, $FeOOH/BiVO_4$, and $FeOOH/Ti:BiVO_4$ are 8.3, 20.4, 25.4, and 43.7% at ~400 nm.

The applied bias photon-to-current conversion efficiencies (ABPEs) were calculated (Figure 4c), where the ABPEs reached a maximum of 0.19, 0.37, 0.51, and 0.81% for $BiVO_4$, $Ti:BiVO_4$, $FeOOH/BiVO_4$, and $FeOOH/Ti:BiVO_4$. In Figure 4d, Tafel curves show that the overpotential of $FeOOH/Ti:BiVO_4$ (556 mA dec^{-1}) is lower than those of $BiVO_4$ (821 mA dec^{-1}), $Ti:BiVO_4$ (646 mA dec^{-1}), and $FeOOH/BiVO_4$ (663 mA dec^{-1}), indicating that $FeOOH/Ti:BiVO_4$ is more favorable to accelerate the OER, corresponding to the slopes of LSV curves.

Charge Transfer Kinetics. To gain insight into the improved PEC performance, the charge transfer mechanism was investigated (Figure 5). The J_{PEC} was obtained from eq 3[32,36]

$$J_{\text{PEC}} = J_{\text{abs}} \times \eta_{\text{bulk}} \times \eta_{\text{surface}} \tag{3}$$

where J_{abs} is the photocurrent density that all absorbed photons (100%) convert to the current density without any recombination, η_{surface} is the surface charge transfer efficiency of photoexcited holes participating in water oxidation, and η_{bulk} is the bulk charge separation efficiency of photogenerated holes and electrons separating.[37,38] Because Na_2SO_3 acts as a scavenger, photoexcited holes are assumed to participate in water oxidation as soon as they arrive at the semiconductor/electrolyte interface without surface recombination (η_{surface} = 100%). Herein, η_{surface} and η_{bulk} are calculated as in eqs 4 and 5

$$\eta_{\text{surface}} \approx J_{\text{PEC}}/J_{\text{Na}_2\text{SO}_3} \tag{4}$$

$$\eta_{\text{bulk}} \approx J_{\text{Na}_2\text{SO}_3}/J_{\text{abs}} \tag{5}$$

where $J_{\text{Na}_2\text{SO}_3}$ and J_{PEC} are measured with or without Na_2SO_3. In Figure 5a, the η_{surface} are 30.7, 39.1, 58.7, and 61.6% at 1.23 V vs RHE for $BiVO_4$, $Ti:BiVO_4$, $FeOOH/BiVO_4$, and $FeOOH/Ti:BiVO_4$. In Figure 5b, the η_{bulk} values are 60.1, 88.3, 68.1, and 90.2% at 1.23 V vs RHE for $BiVO_4$, $Ti:BiVO_4$, $FeOOH/BiVO_4$, and $FeOOH/Ti:BiVO_4$. The η_{bulk} of $Ti:BiVO_4$ (88.3%) is much higher than that of $BiVO_4$ (60.1%), indicating bulk charge separation is promoted by Ti doping. According to Mott–Schottky (MS) plots in Figure S12, the charge carrier density (N_d) of $Ti:BiVO_4$ increases to 5.86×10^{18} cm^{-3}, 1.81 times than 3.24×10^{18} cm^{-3} of $BiVO_4$ for Ti doping.

Electrochemical impedance spectroscopy (EIS) measurements could characterize the charge transfer kinetics. In Figure 5c, the semicircle radii of Nyquist plots are in the order $BiVO_4$ > $Ti:BiVO_4$ > $FeOOH/BiVO_4$ > $FeOOH/Ti:BiVO_4$ with the Randle equivalent circuit, reflecting the holes-to-water resistance.[38,39] Table S2 lists the series resistances (R_s), the interfacial charge transfer resistances (R_{ct}), and the capacitance of the double layer (C_{dl}) fitted by Zsimpwin software. The R_{ct} values of $BiVO_4$, $Ti:BiVO_4$, $FeOOH/BiVO_4$, and $FeOOH/Ti:BiVO_4$ are 1048.0, 399.5, 384.6, and 242.0 Ω, respectively.

https://doi.org/10.1021/acsami.2c23169
ACS Appl. Mater. Interfaces XXXX, XXX, XXX−XXX

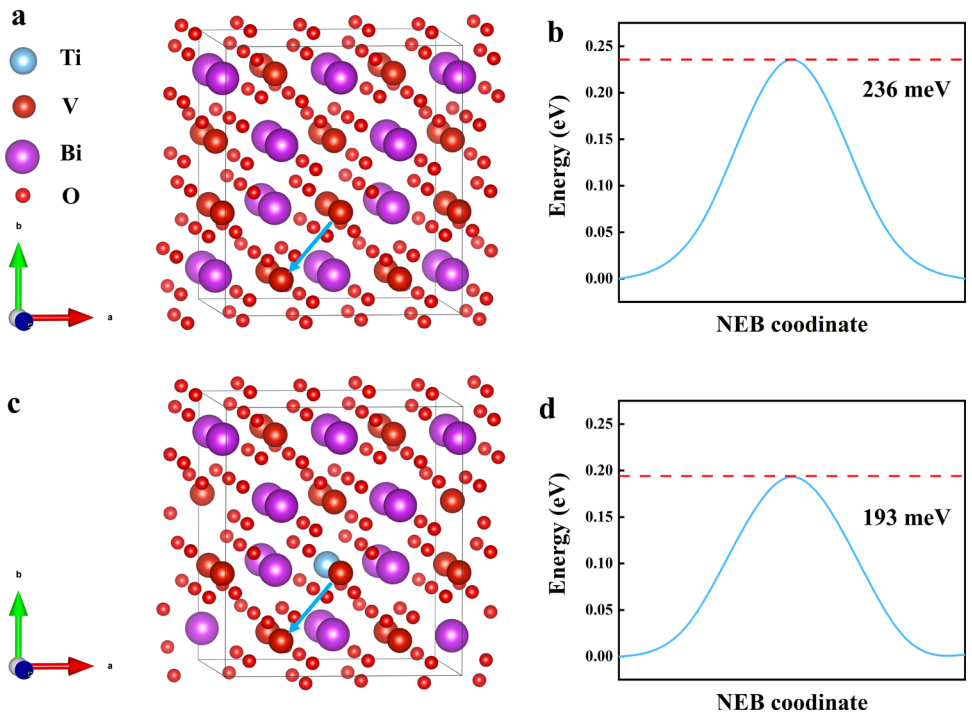

Figure 6. (a, c) Small polaron hopping between two adjacent V sites in the $BiVO_4$ and Ti:$BiVO_4$ for cNEB simulation. (b, d) Hopping activation energy barriers of $BiVO_4$ and Ti:$BiVO_4$.

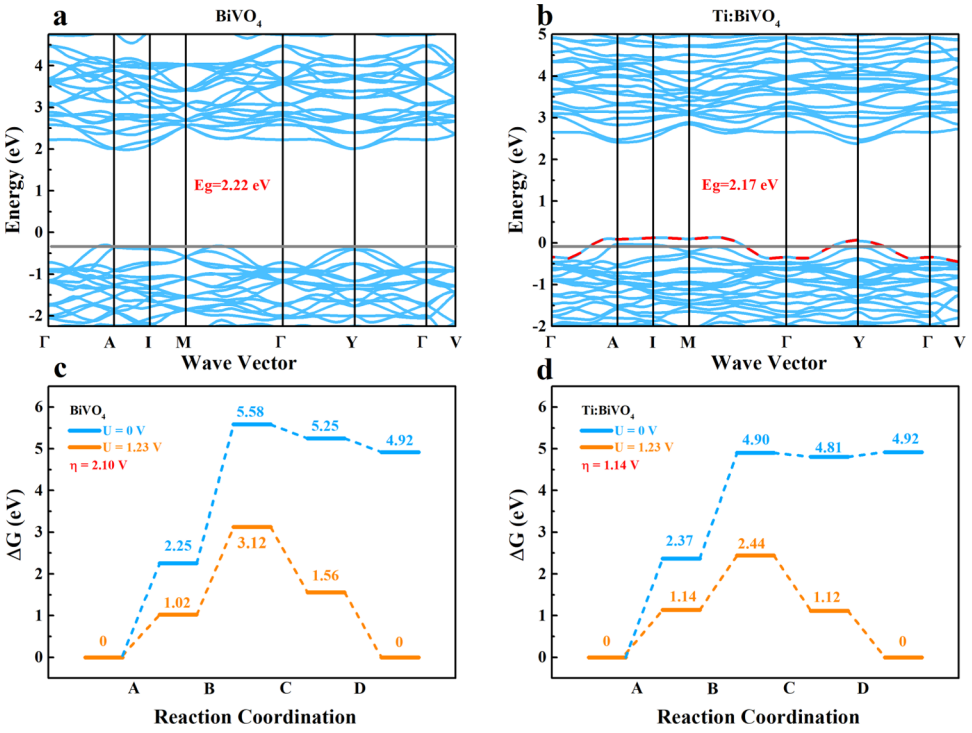

Figure 7. (a, b) Band structure of $BiVO_4$ and Ti:$BiVO_4$ and (c, d) ΔG of the OER for $BiVO_4$ and Ti:$BiVO_4$.

The lowest R_{ct} of FeOOH/Ti:$BiVO_4$ demonstrates the fastest interfacial charge transfer at the electrode/electrolyte interface.[40,41] It indicates that the interfacial transfer kinetics of $BiVO_4$ photoanode is dramatically improved by Ti doping and FeOOH OEC.

The electron collection time (τ_c) could reflect the electron transfer between the semiconductor and the substrate through the IMPS plots (Figure 5d). The frequency (f_{min}) of the imaginary minimum is to calculate τ_c as in eq 6

$$\tau_c = 1/2\pi f_{min} \tag{6}$$

The τ_c of $BiVO_4$, Ti:$BiVO_4$, FeOOH/$BiVO_4$, and FeOOH/Ti:$BiVO_4$ are 16.53, 3.39, 4.32, and 2.12 ms, indicating Ti doping and FeOOH layer promoting the electron transfer from the substrate to FTO. The electron recombination lifetime (τ_r)

https://doi.org/10.1021/acsami.2c23169
ACS Appl. Mater. Interfaces XXXX, XXX, XXX−XXX

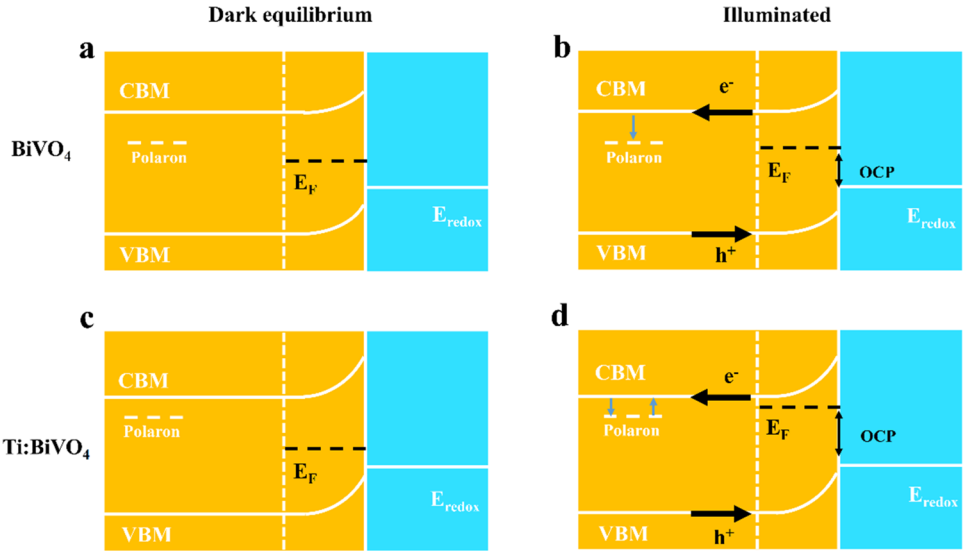

Figure 8. Schematic diagram of the band structures and band bendings for $BiVO_4$ and Ti:$BiVO_4$. (a, c) Dark equilibrium state and (b, d) illuminated state. Adapted and reprinted with permission from Ye, K.-H. et al. Enhancing photoelectrochemical water splitting by combining work function tuning and heterojunction engineering. Nat. Commun. **2019**, 10 (1), 3687. Copyright 2019 Springer Nature.

of $BiVO_4$ and Ti:$BiVO_4$ is measured through the IMVS plots (Figure S13) and calculated as in eq 7

$$\tau_r = 1/2\pi f_{min} \quad (7)$$

where f_{min} is the frequency of the imaginary minimum. The τ_r of Ti:$BiVO_4$ is 0.838 s, much higher than that of $BiVO_4$ (0.116 s), indicating that Ti doping could promote the charge transport of $BiVO_4$ to extend the lifetime of photogenerated carriers.

DFT Calculations. The optimized $BiVO_4$ parameters were consistent with the crystalline phase (JCPDS no. 14-0688), and a 2 × 1 × 2 supercell was built to calculate the polaron hopping barrier for the $BiVO_4$ sample through climbing nudged elastic band (cNEB) simulation. One V site was substituted by Ti to construct the Ti:$BiVO_4$ model. An extra electron is added to form a small polaron with four distorted bonds of V,[42] and the hopping path between two adjacent V sites is illustrated as a blue arrow (Figure 6a,c). In $BiVO_4$, the polaron hopping barrier was calculated to be 236 meV (Figure 6b). However, the hopping barrier in the same hopping path for Ti:$BiVO_4$ was calculated to be 193 meV, lower than that in $BiVO_4$ (Figure 6d). These calculations indicate that Ti doping could promote polaron migration between the two adjacent V sites.[24]

The band structures of $BiVO_4$ and Ti:$BiVO_4$ were obtained (Figure 7a,b) with E_g values of 2.22 and 2.17 eV. Aligned with the band structures of two samples, the red line in Figure 7b is contributed by Ti doping to narrow the E_g of Ti:$BiVO_4$, mainly because of the hybridization of Ti and O 2p states close to the VBM. The UV−vis absorption spectra of $BiVO_4$ and Ti:$BiVO_4$ were carried out from 200 to 800 nm (Figure S14). With the Ti doping, the absorption edge of the Ti:$BiVO_4$ is extended from 499 to 505 nm compared to $BiVO_4$, consistent with the narrowed E_g. The VBM XPS spectra of $BiVO_4$ and Ti:$BiVO_4$ films were measured (Figure S15), where the valence band maximum of Ti:$BiVO_4$ has a negative shift in contrast to $BiVO_4$, corresponding to the upshift of valence bands in Figure 7b.

The Gibbs free energy changes (ΔG) of $BiVO_4$ and Ti:$BiVO_4$ are explored to reflect the energy barrier of the OER steps in Figure 7c,d. In Table S2, free energies of H_2O, H_2, and O_2 as gas are thermally corrected, and free energies of intermediates of $BiVO_4$ and Ti:$BiVO_4$ are corrected by zero-point energies (ZPEs) (Tables S3 and S4). The bare $BiVO_4$ begins from that the ·OH group of gaseous H_2O is absorbed on the Bi site to form *OH as reaction A.[14] Then, *OH transforms to *O as reaction B, and another ·OH group of gaseous H_2O is captured on *O to *OOH. Finally, O_2 is released from the *OOH as reaction D. The ΔG of $BiVO_4$ with four proton transfers is cumulated in Figure 7c, where the maximum ΔG is 3.33 eV for the formation of *O, corresponding to the overpotential (η) of 2.10 V.[43] Similar to the process of $BiVO_4$, Ti:$BiVO_4$ starts from the step of proton transfer from H_2O to an electrolyte, namely, absorption of the ·OH group from gaseous H_2O on Bi sites. Then, the process is taken as the reaction order of A−B−C−D with the cumulative reaction energy in Figure 7d. Here, the maximum ΔG is 2.37 eV for absorption of the ·OH group on Bi sites, so that η is equal to 1.14 V, which is consistent with the overpotentials from the Tafel plots.

In addition, the transient open-circuit potential (OCP) plots (Figure S16) show that the Ti:$BiVO_4$ has a higher photovoltage (0.38 V) than that of pristine $BiVO_4$ (0.25 V), suggesting a stronger thermodynamic driving force for the OER. A schematic diagram of the band structures for $BiVO_4$ and Ti:$BiVO_4$ is illustrated in Figure 8a−d. With the doping of Ti^{4+}, the band bending at the semiconductor/electrolyte interface is strengthened (Figure 8c,d). Moreover, the cNEB simulation results suggest that the polaron hopping energy barrier was reduced by Ti doping, moving the polaron state closer to the conduction band. Under illumination, the photogenerated holes start to transfer to the interface and generated electrons transfer in reverse orientation with increasing OCP. It indicates that Ti doping could enhance light absorption, promote charge transport, strengthen band bending, and enlarge photovoltage.

https://doi.org/10.1021/acsami.2c23169
ACS Appl. Mater. Interfaces XXXX, XXX, XXX−XXX

CONCLUSIONS

In this study, we propose an unconventional substitution of the sites V^{5+} via Ti^{4+} in $BiVO_4$, for the similar ionic radii and accelerated polaron hopping. The synthesized Ti:$BiVO_4$ increases the charge carrier density 1.81 times to 5.86×10^{18} cm^{-3} and increases the photocurrent density 1.90 times up to 2.51 mA cm^{-2}, with the bulk separation efficiency of 88.3% at 1.23 V vs RHE. The DFT calculations have illustrated that the Ti-doping modification could promote polaron hopping, narrow the E_g, and decrease the overpotential concurrently. With further spin-coated FeOOH cocatalyst, the photoanode has a photocurrent density of 3.99 mA cm^{-2} at 1.23 V vs RHE. The improved PEC performance of FeOOH/Ti:$BiVO_4$ is attributed to the synergistic effect of FeOOH OEC and Ti-doping modification.

ASSOCIATED CONTENT

Supporting Information

The Supporting Information is available free of charge at https://pubs.acs.org/doi/10.1021/acsami.2c23169.

DFT method, XRD, XPS, TEM, AFM, photocurrent density, long-term stability, IMVS, UV−vis, VBM XPS, and OCP (PDF)

AUTHOR INFORMATION

Corresponding Authors

Jing Bai − *School of Environmental Science and Engineering, Key Laboratory of Thin Film and Microfabrication Technology (Ministry of Education), Shanghai Jiao Tong University, Shanghai 200240, P. R. China;* orcid.org/0000-0001-6957-190X; Email: bai_jing@sjtu.edu.cn

Baoxue Zhou − *School of Environmental Science and Engineering, Key Laboratory of Thin Film and Microfabrication Technology (Ministry of Education), Shanghai Jiao Tong University, Shanghai 200240, P. R. China; Shanghai Institute of Pollution Control and Ecological Security, Shanghai 200092, P. R. China;* orcid.org/0000-0001-9691-3119; Email: zhoubaoxue@sjtu.edu.cn

Authors

Jiachen Wang − *School of Environmental Science and Engineering, Key Laboratory of Thin Film and Microfabrication Technology (Ministry of Education), Shanghai Jiao Tong University, Shanghai 200240, P. R. China*

Yan Zhang − *School of Environmental Science and Engineering, Key Laboratory of Thin Film and Microfabrication Technology (Ministry of Education), Shanghai Jiao Tong University, Shanghai 200240, P. R. China*

Lei Li − *School of Environmental Science and Engineering, Key Laboratory of Thin Film and Microfabrication Technology (Ministry of Education), Shanghai Jiao Tong University, Shanghai 200240, P. R. China;* orcid.org/0000-0003-4909-5904

Changhui Zhou − *School of Environmental Science and Engineering, Key Laboratory of Thin Film and Microfabrication Technology (Ministry of Education), Shanghai Jiao Tong University, Shanghai 200240, P. R. China*

Tingsheng Zhou − *School of Environmental Science and Engineering, Key Laboratory of Thin Film and Microfabrication Technology (Ministry of Education), Shanghai Jiao Tong University, Shanghai 200240, P. R. China*

Jinhua Li − *School of Environmental Science and Engineering, Key Laboratory of Thin Film and Microfabrication Technology (Ministry of Education), Shanghai Jiao Tong University, Shanghai 200240, P. R. China*

Hong Zhu − *University of Michigan—Shanghai Jiao Tong University Joint Institute, Shanghai Jiao Tong University, Shanghai 200240, P. R. China;* orcid.org/0000-0001-7919-5661

Complete contact information is available at: https://pubs.acs.org/10.1021/acsami.2c23169

Notes

The authors declare no competing financial interest.

ACKNOWLEDGMENTS

The authors acknowledge the National Key Research and Development Program of China (2018YFE0122300), National Nature Science Foundation of China (Nos. 22076121 and 22206213), and SJTU-AEMD and SJTU Center for High Performance Computing for support.

REFERENCES

(1) Park, Y.; McDonald, K. J.; Choi, K. S. Progress in Bismuth Vanadate Photoanodes for Use in Solar Water Oxidation. *Chem. Soc. Rev.* **2013**, *42*, 2321−2337.

(2) Chi, J.; Jiang, Z.; Yan, J.; Larimi, A.; Wang, Z.; Wang, L.; Shangguan, W. Recent Advancements in Bismuth Vanadate Photoanodes for Photoelectrochemical Water Splitting. *Mater. Today Chem.* **2022**, *26*, 101060−101100.

(3) Pan, J. B.; Shen, S.; Chen, L.; Au, C. T.; Yin, S. F. Core−Shell Photoanodes for Photoelectrochemical Water Oxidation. *Adv. Funct. Mater.* **2021**, *31*, No. 2104269.

(4) Luo, W.; Yang, Z.; Li, Z.; Zhang, J.; Liu, J.; Zhao, Z.; Wang, Z.; Yan, S.; Yu, T.; Zou, Z. Solar Hydrogen Generation from Seawater with a Modified $BiVO_4$ Photoanode. *Energy Environ. Sci.* **2011**, *4*, 4046−4051.

(5) Abdi, F. F.; Savenije, T. J.; May, M. M.; Dam, B.; van de Krol, R. The Origin of Slow Carrier Transport in $BiVO_4$ Thin Film Photoanodes: A Time-Resolved Microwave Conductivity Study. *J. Phys. Chem. Lett.* **2013**, *4*, 2752−2757.

(6) Zhang, Y.; Bai, J.; Wang, J.; Chen, S.; Zhu, H.; Li, J.; Li, L.; Zhou, T.; Zhou, B. In-Situ and Synchronous Generation of Oxygen Vacancies and FeO_x OECs on $BiVO_4$ for Ultrafast Electron Transfer and Excellent Photoelectrochemical Performance. *Chem. Eng. J.* **2020**, *401*, No. 126134.

(7) Yin, X.; Li, J.; Du, L.; Zhan, F.; Kawashima, K.; Li, W.; Qiu, W.; Liu, Y.; Yang, X.; Wang, K.; Ning, Y.; Mullins, C. B. Boosting Photoelectrochemical Performance of $BiVO_4$ through Photoassisted Self-Reduction. *ACS Appl. Energy Mater.* **2020**, *3*, 4403−4410.

(8) Pan, J. B.; Wang, B. H.; Wang, J. B.; Ding, H. Z.; Zhou, W.; Liu, X.; Zhang, J. R.; Shen, S.; Guo, J. K.; Chen, L.; Au, C. T.; Jiang, L. L.; Yin, S. F. Activity and Stability Boosting of an Oxygen-Vacancy-Rich $BiVO_4$ Photoanode by Nife-MOFs Thin Layer for Water Oxidation. *Angew. Chem., Int. Ed.* **2021**, *60*, 1433−1440.

(9) Zhang, B.; Wang, L.; Zhang, Y.; Ding, Y.; Bi, Y. Ultrathin FeOOH Nanolayers with Abundant Oxygen Vacancies on $BiVO_4$ Photoanodes for Efficient Water Oxidation. *Angew. Chem., Int. Ed.* **2018**, *57*, 2248−2252.

(10) Zhou, T.; Wang, J.; Zhang, Y.; Zhou, C.; Bai, J.; Li, J.; Zhou, B. Oxygen Vacancy-Abundant Carbon Quantum Dots as Superfast Hole Transport Channel for Vastly Improving Surface Charge Transfer Efficiency of $BiVO_4$ Photoanode. *Chem. Eng. J.* **2022**, *431*, No. 133414.

(11) Zhong, M.; Hisatomi, T.; Kuang, Y.; Zhao, J.; Liu, M.; Iwase, A.; Jia, Q.; Nishiyama, H.; Minegishi, T.; Nakabayashi, M.; Shibata, N.; Niishiro, R.; Katayama, C.; Shibano, H.; Katayama, M.; Kudo, A.; Yamada, T.; Domen, K. Surface Modification of CoO_x Loaded $BiVO_4$ Photoanodes with Ultrathin P-Type NiO Layers for Improved Solar Water Oxidation. *J. Am. Chem. Soc.* **2015**, *137*, 5053−5060.
(12) Eisenberg, D.; Ahn, H. S.; Bard, A. J. Enhanced Photoelectrochemical Water Oxidation on Bismuth Vanadate by Electrodeposition of Amorphous Titanium Dioxide. *J. Am. Chem. Soc.* **2014**, *136*, 14011−14014.
(13) Wang, J.; Zhou, T.; Zhang, Y.; Li, L.; Zhou, C.; Bai, J.; Li, J.; Zhu, H.; Zhou, B. Type-II Heterojunction $CdIn_2S_4/BiVO_4$ Coupling with CQDs to Improve PEC Water Splitting Performance Synergistically. *ACS Appl. Mater. Interfaces* **2022**, *14*, 45392−45402.
(14) Pan, Q.; Yang, K.; Wang, G.; Li, D.; Sun, J.; Yang, B.; Zou, Z.; Hu, W.; Wen, K.; Yang, H. $BiVO_4$ Nanocrystals with Controllable Oxygen Vacancies Induced by Zn-doping Coupled with Graphene Quantum Dots for Enhanced Photoelectrochemical Water Splitting. *Chem. Eng. J.* **2019**, *372*, 399−407.
(15) Yang, X.; Fernandez-Carrion, A. J.; Wang, J.; Porcher, F.; Fayon, F.; Allix, M.; Kuang, X. Cooperative Mechanisms of Oxygen Vacancy Stabilization and Migration in the Isolated Tetrahedral Anion Scheelite Structure. *Nat. Commun.* **2018**, *9*, No. 4484.
(16) Kim, J. K.; Shi, X.; Jeong, M. J.; Park, J.; Han, H. S.; Kim, S. H.; Guo, Y.; Heinz, T. F.; Fan, S.; Lee, C. L.; Park, J. H.; Zheng, X. Enhancing Mo:$BiVO_4$ Solar Water Splitting with Patterned Au Nanospheres by Plasmon-Induced Energy Transfer. *Adv. Energy Mater.* **2018**, *8*, No. 1701765.
(17) Zhong, X.; He, H.; Yang, M.; Ke, G.; Zhao, Z.; Dong, F.; Wang, B.; Chen, Y.; Shi, X.; Zhou, Y. In^{3+}-Doped $BiVO_4$ Photoanodes with Passivated Surface States for Photoelectrochemical Water Oxidation. *J. Mater. Chem. A* **2018**, *6*, 10456−10465.
(18) Gutkowski, R.; Peeters, D.; Schuhmann, W. Improved Photoelectrochemical Performance of Electrodeposited Metal-Doped $BiVO_4$ on Pt-Nanoparticle Modified FTO Surfaces. *J. Mater. Chem. A* **2016**, *4*, 7875−7882.
(19) Ye, K. H.; Li, H.; Huang, D.; Xiao, S.; Qiu, W.; Li, M.; Hu, Y.; Mai, W.; Ji, H.; Yang, S. Enhancing Photoelectrochemical Water Splitting by Combining Work Function Tuning and Heterojunction Engineering. *Nat. Commun.* **2019**, *10*, No. 3687.
(20) Abdi, F. F.; Han, L.; Smets, A. H.; Zeman, M.; Dam, B.; van de Krol, R. Efficient Solar Water Splitting by Enhanced Charge Separation in a Bismuth Vanadate-Silicon Tandem Photoelectrode. *Nat. Commun.* **2013**, *4*, No. 2195.
(21) Zhang, L.; Lin, C. Y.; Valev, V. K.; Reisner, E.; Steiner, U.; Baumberg, J. J. Plasmonic Enhancement in $BiVO_4$ Photonic Crystals for Efficient Water Splitting. *Small* **2014**, *10*, 3970−3978.
(22) Jo, W. J.; Jang, J. W.; Kong, K. J.; Kang, H. J.; Kim, J. Y.; Jun, H.; Parmar, K. P.; Lee, J. S. Phosphate Doping into Monoclinic $BiVO_4$ for Enhanced Photoelectrochemical Water Oxidation Activity. *Angew. Chem., Int. Ed.* **2012**, *51*, 3147−3151.
(23) Wu, H.; Zhang, L.; Du, A.; Irani, R.; van de Krol, R.; Abdi, F. F.; Ng, Y. H. Low-Bias Photoelectrochemical Water Splitting Via Mediating Trap States and Small Polaron Hopping. *Nat. Commun.* **2022**, *13*, No. 6231.
(24) Zhang, W.; Wu, F.; Li, J.; Yan, D.; Tao, J.; Ping, Y.; Liu, M. Unconventional Relation between Charge Transport and Photocurrent Via Boosting Small Polaron Hopping for Photoelectrochemical Water Splitting. *ACS Energy Lett.* **2018**, *3*, 2232−2239.
(25) Peng, B.; Shi, Y.; Zhang, X.; Lv, P. Top-Down Fabrication of Ti Doped $BiVO_4$ Nanosheets for Efficient Water Oxidation under Visible Light. *Catal. Sci. Technol.* **2021**, *11*, 7898−7904.
(26) Khanh Huyen, N. T.; Pham, T.-D.; Dieu Cam, N. T.; Van Quan, P.; Van Noi, N.; Hanh, N. T.; Thanh Tung, M. H.; Dao, V.-D. Fabrication of Titanium Doped $BiVO_4$ as a Novel Visible Light Driven Photocatalyst for Degradation of Residual Tetracycline Pollutant. *Ceram. Int.* **2021**, *47*, 34253−34259.
(27) Luo, H.; Liu, C.; Xu, Y.; Zhang, C.; Wang, W.; Chen, Z. An Ultra-Thin NiOOH Layer Loading on $BiVO_4$ Photoanode for Highly Efficient Photoelectrochemical Water Oxidation. *Int. J. Hydrogen Energy* **2019**, *44*, 30160−30170.
(28) Feng, J.; Bian, J.; Bai, L.; Xi, S.; Wang, Y.; Chen, C.; Jing, L. Efficient Wide-Spectrum Photocatalytic Overall Water Splitting over Ultrathin Molecular Nickel Phthalocyanine/$BiVO_4$ Z-Scheme Heterojunctions without Noble Metals. *Appl. Catal., B* **2021**, *295*, No. 120260.
(29) Zhou, T.; Li, L.; Li, J.; Wang, J.; Bai, J.; Xia, L.; Xu, Q.; Zhou, B. Electrochemically Reduced TiO_2 Photoanode Coupled with Oxygen Vacancy-Rich Carbon Quantum Dots for Synergistically Improving Photoelectrochemical Performance. *Chem. Eng. J.* **2021**, *425*, No. 131770.
(30) Pan, J.-B.; Liu, X.; Wang, B.-H.; Chen, Y.-A.; Tan, H.-Y.; Ouyang, J.; Zhou, W.; Shen, S.; Chen, L.; Au, C.-T.; Yin, S.-F. Conductive MOFs Coating on Hematite Photoanode for Activity Boost Via Surface State Regulation. *Appl. Catal., B* **2022**, *315*, No. 121526.
(31) Bao, S.; Wang, Z.; Zhang, J.; Tian, B. Facet-Heterojunction-Based Z-Scheme $BiVO_4$ {010} Microplates Decorated with AgBr-Ag Nanoparticles for the Photocatalytic Inactivation of Bacteria and the Decomposition of Organic Contaminants. *ACS Appl. Nano Mater.* **2020**, *3*, 8604−8617.
(32) Zhou, T.; Chen, S.; Li, L.; Wang, J.; Zhang, Y.; Li, J.; Bai, J.; Xia, L.; Xu, Q.; Rahim, M.; Zhou, B. Carbon Quantum Dots Modified Anatase/Rutile TiO_2 Photoanode with Dramatically Enhanced Photoelectrochemical Performance. *Appl. Catal., B* **2020**, *269*, No. 118776.
(33) Hu, J.; Zhang, S.; Cao, Y.; Wang, H.; Yu, H.; Peng, F. Novel Highly Active Anatase/Rutile TiO_2 Photocatalyst with Hydrogenated Heterophase Interface Structures for Photoelectrochemical Water Splitting into Hydrogen. *ACS Sustainable Chem. Eng.* **2018**, *6*, 10823−10832.
(34) Wang, J.; Zhou, T.; Zhang, Y.; Chen, S.; Bai, J.; Li, J.; Zhu, H.; Zhou, B. The Design of High Performance Photoanode of CQDs/TiO_2/WO_3 Based on DFT Alignment of Lattice Parameter and Energy Band, and Charge Distribution. *J. Colloid Interface Sci.* **2021**, *600*, 828−837.
(35) Cai, L.; Zhao, J.; Li, H.; Park, J.; Cho, I. S.; Han, H. S.; Zheng, X. One-Step Hydrothermal Deposition of Ni:FeOOH onto Photoanodes for Enhanced Water Oxidation. *ACS Energy Lett.* **2016**, *1*, 624−632.
(36) Kim, T. W.; Choi, K.-S. Nanoporous $BiVO_4$ Photoanodes with Dual-Layer Oxygen Evolution Catalysts for Solar Water Splitting. *Science* **2014**, *343*, 990−994.
(37) Kim, J. H.; Lee, J. S. Elaborately Modified $BiVO_4$ Photoanodes for Solar Water Splitting. *Adv. Mater.* **2019**, *31*, No. 1806938.
(38) Yang, G.; Li, Y.; Pang, H.; Chang, K.; Ye, J. Ultrathin Cobalt−Manganese Nanosheets: An Efficient Platform for Enhanced Photoelectrochemical Water Oxidation with Electron-Donating Effect. *Adv. Funct. Mater.* **2019**, *29*, No. 1904622.
(39) Ye, K.-H.; Wang, Z.; Gu, J.; Xiao, S.; Yuan, Y.; Zhu, Y.; Zhang, Y.; Mai, W.; Yang, S. Carbon Quantum Dots as a Visible Light Sensitizer to Significantly Increase the Solar Water Splitting Performance of Bismuth Vanadate Photoanodes. *Energy Environ. Sci.* **2017**, *10*, 772−779.
(40) Upul Wijayantha, K. G.; Saremi Yarahmadi, S.; Peter, L. M. Kinetics of Oxygen Evolution at alpha-Fe_2O_3 Photoanodes: A Study by Photoelectrochemical Impedance Spectroscopy. *Phys. Chem. Chem. Phys.* **2011**, *13*, 5264−5270.
(41) Valdés, Á.; Qu, Z.; Kroes, G.; Rossmeisl, J.; Nørskov, J. K. Oxidation and Photo-Oxidation of Water on TiO_2 Surface. *J. Phys. Chem. C* **2008**, *112*, 9872−9879.
(42) Lee, D.; Baltazar, V. U.; Smart, T. J.; Ping, Y.; Choi, K. S. Electrochemical Oxidation of Metal-Catechol Complexes as a New Synthesis Route to the High-Quality Ternary Photoelectrodes: A Case Study of Fe_2TiO_5 Photoanodes. *ACS Appl. Mater. Interfaces* **2020**, *12*, 29275−29284.
(43) Wang, Z.; Mao, X.; Chen, P.; Xiao, M.; Monny, S. A.; Wang, S.; Konarova, M.; Du, A.; Wang, L. Understanding the Roles of Oxygen

https://doi.org/10.1021/acsami.2c23169
ACS Appl. Mater. Interfaces XXXX, XXX, XXX−XXX

Vacancies in Hematite-Based Photoelectrochemical Processes. *Angew. Chem., Int. Ed.* **2019**, *58*, 1030−1034.

https://doi.org/10.1021/acsami.2c23169
ACS Appl. Mater. Interfaces XXXX, XXX, XXX−XXX